Diffraction of real and virtual photons in a pyrolytic graphite crystal as source of intensive quasimonochromatic X-ray beam

E.A. Bogomazova *, B.N. Kalinin, G.A. Naumenko, D.V. Padalko, A.P. Potylitsyn, A.F. Sharafutdinov, I.E. Vnukov

Nuclear Physics Institute, Tomsk Polytechnic University, P.O. Box 25, Lenin Avenue 2-a, 634050 Tomsk, Russia

Received 14 March 2002; received in revised form 1 August 2002

Abstract

A series of experiments on the parametric X-rays radiation (PXR) generation and radiation soft component diffraction of relativistic electrons in pyrolytic graphite (PG) crystals have been carried out at the Tomsk synchrotron. It is shown that the experimental results with PG crystals are explained by the kinematic PXR theory if we take into account a contribution of the real photons diffraction (transition radiation, bremsstrahlung and PXR photons as well). The measurements of the emission spectrum of channeled electrons in the photon energy range much smaller than the characteristic energy of channeling radiation have been performed with a crystal-diffraction spectrometer. For electrons incident along the $\langle 1\,1\,0\rangle$ axis of a silicon crystal, the radiation intensity in the energy range $30 \leqslant \omega \leqslant 360$ keV exceeds the bremsstrahlung one almost by an order of magnitude. Different possibilities to create an effective source of the monochromatic X-ray beam based on the real and virtual photons diffraction in the PG crystals have been considered.

Keywords: Parametric X-ray radiation; Diffracted radiation; Channeling radiation; Pyrolytic graphite crystal

1. Introduction

Intensive monochromatic and tunable X-ray beams are extensively exploited in applied investigations, industry and medicine. As a rule, these devices are based on a primary powerful radiation source and crystal monochromator. Different radiation mechanisms are used – bremsstrahlung from X-ray tube, synchrotron (SR) and an undulator radiation (UR).

The parametric X-rays radiation (PXR), that can be treated as the own field diffraction of a fast charged particle moving through a crystal, and diffracted γ-radiation which are intrinsically monochromatic and readily tunable may be considered as an alternative source of a monochromatic X-ray beam. For moderate electron energies ($E_0 \leqslant 1$ GeV) and X-ray range of photon energies (20–300 keV), the radiation intensities from a

* Corresponding author.
E-mail address: bgm@npi.tpu.ru (E.A. Bogomazova).

condensed matter target (such as bremsstrahlung, channeling radiation, transition radiation, PXR) are much greater compared to the SR and UR intensities.

Mosaic pyrolytic graphite (PG) crystals are known to have the highest X-ray reflectivity in comparison with other crystals [1]. The X-ray diffraction theory in mosaic crystals is consistent with the experimental results obtained with PG crystals [2]. However, the PXR yield measurements in a PG crystal [3] have shown that measured ratio of intensities of the different reflection orders differs greatly from the calculated one. In our previous measurements with a pyrolytic graphite crystal [4] we experimentally demonstrated that for electrons with energy $E_0 = 850$ MeV and photons energy $\omega \sim \gamma\omega_p$, where γ is Lorentz factor, ω_p is plasmon energy of medium, the contribution of bremsstrahlung photons diffraction to the spectrum measured was comparable to the PXR yield and depended significantly on the spectral and angular distribution of radiation generated in the crystal.

The PXR experimental investigations in mosaic pyrolytic graphite crystals under the same experimental conditions but in different spectral ranges ($\omega \ll \gamma\omega_p$ and $\omega > \gamma\omega_p$) with allowance for contributions of the real photons diffraction may elucidate a physical reason for the large discrepancy between prediction of kinematic PXR theory and results of the previous experiments [3,4]. On the other hand, mosaic pyrolytic graphite crystals, known for their high X-ray reflectivity and used as targets for PXR generation, may ensure much higher radiation yield compared to conventionally used diamond, silicon, and germanium monocrystals.

It is well known (see for example [5,6]) that for electrons with energies of the order of 1 GeV in the range $\omega \sim \omega_m \approx \omega_0\gamma^{3/2}$ ($\omega_0 \sim 10^2$ eV) the electrons channeling radiation (CR) is the most intensive one compared to other radiation types. As a rule, the main attention in experiments and calculations was given to this range of photon energies. Up to now, experimental investigations of softer part of CR ($\omega \leqslant 0.1\omega_m$) have not yet been performed.

In this range of photon energies, the formation length, or the coherence length ($l_c^0 = \gamma^2\lambda$, where λ is the wavelength) becomes a macroscopic quantity for a photon emitted in the straightforward direction [7] and the spectral and angular distribution of radiation in a dense medium are significantly modified. The bremsstrahlung is suppressed because of the polarization of the medium and the Landau–Pomeranchuk–Migdal effect [8] observed recently in [9,10] for the whole radiation cone and electrons with energies between 8 and 25 GeV.

These effects should be also expected for the particles with lower energies, but in the X-ray energy range $\omega \leqslant 100$ keV. The influence of the medium polarization on the emission spectrum from channeled electrons in crystals has not yet been studied experimentally.

2. Calculation

To calculate the PXR characteristics we used the following formula of spectral and angular PXR distribution derived within kinematic approximation in [11]:

$$\frac{d^2N}{d\iota d\Omega} = \frac{\sum_\alpha \alpha\omega^3 |\chi_{\vec{g}}|^2}{2\pi\varepsilon_0^{3/2}\beta(1-\sqrt{\varepsilon_0}\vec{\beta}\vec{n})} \times \left[\frac{(\omega\vec{\beta}-\vec{g})\vec{e}_{\vec{k}\alpha}}{(\vec{k}_\perp+\vec{g}_\perp)^2 + \frac{\omega^2}{\beta^2}\{\gamma^{-2}+\beta^2(1-\varepsilon_0)\}}\right]^2. \quad (1)$$

The system of units used hereinafter is $\hbar = m_e = c = 1$. Here, $\varepsilon_0 = 1 - \omega^2/\omega_p^2$ is the mean value of the dielectric function, ω_p is the plasmon energy of medium, $\vec{\beta} = \beta\vec{n}_0$ is the electron velocity vector, $\vec{n}_0$ and $\vec{n}$ are the individual vectors corresponding to the incident electron and emitted photon (with the energy ω and momentum $\vec{k}$), $\vec{g}$ is the reciprocal lattice vector, $\vec{e}_{\vec{k}\alpha}$ are the polarization vectors, $\perp$ is the index denoting the vector projections on the plane normal to $\vec{n}_0$. The remaining notations are conventional. The term $|\chi_{\vec{g}}|^2$ denotes the following value:

$$|\chi_{\vec{g}}|^2 = |S(\vec{g})|^2 \exp(-2\langle u_\perp^2\rangle\vec{g}^2)\left[-\frac{\omega_p^2}{\omega^2}\frac{f(\vec{g})}{z}\right]^2. \quad (2)$$

Here, $|S(\vec{g})|^2$ is the structure factor, $\exp(-2\langle u_\perp^2\rangle \vec{g}^2)$ is the Debye–Waller factor for a pyrolytic graphite crystal [2], where $\langle u_\perp^2\rangle$ is the mean-square amplitude of vibration of the carbon atoms perpendicular to the reflecting planes of PG crystals, $f(\vec{g})$ is the Fourier component of the spatial distribution of electrons in a crystal atom ($f(0) = z$ where z is the number of electrons in the atom).

The electron beam divergence and the PXR photon absorption inside the crystal are considered as follows. The crystal is subdivided into a great number of layers. The angular distribution of the electrons inside each layer is determined by the multiple electrons scattering in all layers before it. This distribution, in turn, is used to calculate the PXR spectrum generated in this layer. The PXR absorption is determined by the remaining part of the crystal. The mosaic crystal structure is taken into consideration through calculation of the spectra for different mosaic bulks with allowance for their distribution over the target.

The procedure for calculating the mosaic crystal reflectivity described in [2] was obtained for a monodirect and monoenergetic photon beam. As a rule, a divergent photons beam with a continuous energy spectrum is incident on the crystal. We proceeded from the formula for the reflection of a monodirect and monoenergetic photon beam from an element of the mosaic crystal of volume ΔV [12],

$$\int P(\theta)\,\mathrm{d}\theta = Q\Delta V, \tag{3}$$

where $P(\theta)$ is the reflectivity of the crystal element at an angle θ. According to [2] the reflectivity is proportional to the distribution of mosaic blocks. Here

$$Q = \left(\frac{\mathrm{e}^2}{mc^2}\right)^2 \frac{N^2\lambda^3}{\sin 2\Theta}|F_\mathrm{p}||F(g)|^2, \tag{4}$$

where N is the concentration of scattering centers, $|F(\vec{g})|^2 = 16|f(\vec{g})|^2\exp(-2\langle u_\perp^2\rangle\vec{g}^2)$, λ is the wavelength, $\exp(-2\langle u_\perp^2\rangle\vec{g}^2)$ and $f(\vec{g})$ are the same as in Eq. (2), $|F_\mathrm{p}|$ is the polarization factor which depends on the polarization of radiation incident on the crystal. If the polarization vector is perpendicular to the diffraction plane, $|F_\mathrm{p}| = 1$; otherwise $|F_\mathrm{p}| = \cos^2 2\Theta_\mathrm{B}$. For an unpolarized photon beam $|F_\mathrm{p}| = (1 + \cos^2 2\Theta_\mathrm{B})/2$. Here Θ_B is the angle between the crystallographic plane and the average direction of photon beam propagation.

Let the radiation with the spectral and angular intensity distribution $I(\omega, \vec{n})$ be incident on a mosaic crystal possessing the distribution of reciprocal lattice vectors $P(\vec{g})$ where ω and $\vec{n}$ are the energy and the unit vector directed along the photon momentum vector, respectively. Here $\vec{g} = |\vec{g}|\vec{\alpha}$, where $\vec{\alpha}$ is the unit vector specifying the deflection of crystal microblocks from the average direction $\vec{g}_0 = \langle\vec{g}\rangle$. The vector $\vec{g}_0$ is perpendicular to a crystal plane. It is rotated through the angle $(\pi/2 - \Theta_\mathrm{B})$ about the beam axis. The diffraction plane is determined by vectors $\vec{n}_0$ and $\vec{g}$.

Based on Bragg's law for a photon with energy ω and propagation direction $\vec{n}$, we can write the following requirement imposed on the direction of vector $\vec{g}$ of the microblock on which the photon can diffract:

$$\omega = \frac{\vec{g}\vec{n}}{\sqrt{\varepsilon_0}(1 - \vec{n}'\vec{n})} = \frac{|\vec{g}|\sin\Theta}{\sqrt{\varepsilon_0}(1 - \cos 2\Theta)}, \tag{5}$$

where $\vec{n}'$ is the vector specifying the direction of the diffracted photon. Hence it follows that the angle between vectors $\vec{n}$ and $\vec{g}$ must meet the condition

$$\sin\Theta = \frac{|\vec{g}|}{2\omega\sqrt{\varepsilon_0}}. \tag{6}$$

A number of mosaic crystal blocks that satisfy the equation

$$\sin\Theta = \frac{(\vec{g}\vec{n})}{|\vec{g}|} = \frac{[n_x g_x + n_y g_y + n_z g_z]}{|\vec{g}|} \tag{7}$$

meet this requirement. From here one can determine the mosaic blocks on which this photon can diffract and the direction of the reflected photon propagation n'.

Then the density of the reflection probability of the photon with fixed ω and $\vec{n}$ in a mosaic crystal block of thickness Δt in the direction of photon propagation can be written as

$$f(\omega, \vec{n}) = q(\omega, \vec{n})Q(\omega)\Delta t, \tag{8}$$

where $q(\omega, \vec{n})$ is the coefficient taking into account the mosaic crystal structure,

$$q(\omega, \vec{n}) = \int P_\mathrm{m}(\alpha_x(\omega, \vec{n}, \alpha_y), \alpha_y)\,\mathrm{d}\alpha_y. \tag{9}$$

Here $P_m(\alpha_x,\alpha_y)$ is the mosaicity distribution in terms of ω, $\vec{n}$, α_x and α_y given by Eqs. (5)–(8).

To calculate the yield of diffracted photons passing through the collimator aperture for the ith reflection order, we took the convolution of the spectral and angular distribution of the radiation intensity $I(\omega,\vec{n})$ with the diffraction probability density over all variables (including energy, angles of photon incidence θ_x and θ_y, and the crystal thickness),

$$dY_i = \int_{\Delta\omega_i} d\omega \int_T dt \iint_{\Delta\Omega} I\left(\omega,\vec{n}\right) Q(\omega) \times q\left(\omega,\vec{n},\vec{n}'\right) d\theta_x d\theta_y, \quad (10)$$

where T is the crystal thickness, $\Delta\Omega$ is the angular acceptance, and $\Delta\omega_i$ is the energy acceptance of the spectrometer for the ith diffraction order.

In our calculations we took into account the experimentally measured mosaic crystal structure distribution (see below) and the extinction of the initial photon beam due to the absorption and diffraction in the crystal (the secondary extinction effect [12]). The secondary diffraction of the reflected photon in the direction of the initial beam propagation from the reflection region to the exit from the crystal was calculated using the formula analogous to Eq. (10) with allowance for the change of the polarization of the radiation diffracted. Numerical values of $f(\vec{g})$, concentration of reflecting centers N and the Debye–Waller factor used in our calculations were taken from [2]. The difference between the values of the crystal reflectivity calculated by the suggested procedure for the monodirectional and monoenergetic photon beam and by the procedure described in [2] did not exceed a few percents.

The calculation error is determined by the errors in measuring the mosaic crystals structure, specifying the PG crystals parameters and employed approximations. We believe that its total value does not exceed 10–15%. The calculation methods of PXR and the γ-radiation diffraction yields in mosaic crystals have been described in details in [13] and [14], respectively.

3. Experimental investigations

3.1. Experimental methods and technique

The experimental study of the PXR spectral characteristics in pyrolytic graphite crystals were carried out with the internal electron beam of the Tomsk synchrotron with electron energies of 500–900 MeV. Fig. 1(a) shows the chart of the experiment. The electrons accelerated to final energy hit a pyrolytic graphite target (PG) placed in a

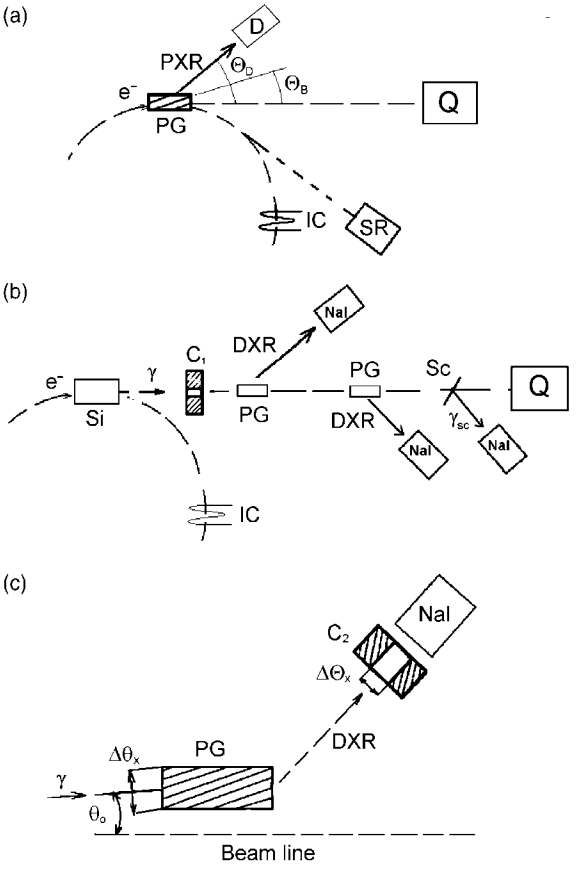

Fig. 1. Schematic layout of experiment: Q – quantometer; PG – pyrolytic graphite crystal; D – detector; IC – inductance current gauge; SR – synchrotron radiation detector; Si – silicon crystal; C_1 – collimator of the bremsstrahlung beam; Sc – scatterer; C_2 – collimator of the diffracted beam; θ_o – observation angle; $\Delta\theta_x$ and $\Delta\Theta_x$ – acceptance of the diffractometer and collimator aperture in the horizontal plane. (a) PXR characteristics measurements; (b) soft radiation component measurements; (c) diffractometer layout.

goniometer. The spectrum and the angular distribution of the emitted radiation were measured by the detector D enclosed in a lead shield. The detector was placed at an angle Θ_D with respect to the electron beam direction. The total energy of bremsstrahlung from the target was measured using the Gauss quantometer Q.

To limit the multitraversal of electrons through a thin internal target an additional target – scraper in the synchrotron can be used [15]. The using of the scraper in the Tomsk synchrotron has allowed us to obtain an average value of the multitraversal about unity [16]. During the spectral measurements the electron beam current was decreased to $\sim 10^6$ particles per pulse and was measured using a synchrotron radiation (SR) detector. For each spill ($\sim$10–15 ms) the number of events detected was of the order of 30–50, and the pile-up probability did not exceed 3–5%. The readings of the synchrotron radiation detector were normalized to absolute values through measurements of the bremsstrahlung total energy from the target under low (SR detector) and high (inductance current gauge (ID)) electron beam currents for the same target orientation. The normalization error was lower than 10–15%.

The measurements were carried out for two PXR emission angles: $\Theta_D = 90°$ ($\omega \ll \gamma\omega_p$) and $\Theta_D = 4°$ ($\omega > \gamma\omega_p$). Because of significant difference in geometry of the measurements, two crystals with dimensions $1 \times 6 \times 10$ mm^3 and $2.5 \times 6.5 \times 22$ mm^3 were used for $\Theta_D = 90°$ and $\Theta_D = 4°$, respectively. The (0 0 2) crystallographic planes of both crystals were nearly parallel to the large face of the targets. During the measurements the crystals were rotated around the electron beam propagation direction through 45° and 2°, respectively.

Both crystals were prepared using the Union Carbide technology, i.e. the same technology as used for preparing targets in the experiment [3]. The mosaic structure of the crystal with dimensions $1 \times 6 \times 10$ mm^3 ($\sigma_m = 3.3 \pm 0.3$ mrad) was measured with an X-ray diffractometer. The diffraction measurements of bremsstrahlung photons in the crystal $2.5 \times 6.5 \times 22$ mm^3 [14] showed that its mosaic structure distribution can be represented as the sum of two Gauss distributions with parameters $\sigma_m = 4.2 \pm 0.1$ mrad, $S_1 \sim 0.67$ and $\sigma_m = 9.0 \pm 0.5$ mrad, $S_2 \sim 0.33$, where σ_m and S are the variance and the weighting coefficient, respectively. The distribution centers coincide with an accuracy better than 0.2 mrad.

For the PXR emission angle $\Theta_D = 90°$ the measurements were carried out for electrons energy of 900 MeV by means of a proportional xenon-filled counter having the efficiency $f \sim 80\%$ at photon energy $\omega \sim 7$ keV and energy resolution $\Delta\omega/\omega \sim 15\%$. The counter was shifted in vertical and horizontal directions to find the PXR reflex center and to measure the PXR angular distribution. The counter was placed at a distance of 116 cm from the crystal. The beam collimation angle $\vartheta_c^{PXR} = 1.74$ mrad was less than the PXR emission characteristic angle $\Theta_{ph} = (\gamma^{-2} + \omega_p^2/\omega^2)^2$. Curve 1 in Fig. 2(a) shows a typical spectrum measured at the center of reflex. The spectrum generated by the electrons passing through an amorphous carbon target of nearly the same thickness was used as the background one (curve 2).

A NaI(Tl) detector with dimensions $\varnothing\ 63 \times 63$ mm^3 was used as a spectrometer for the PXR emission angle $\Theta_D = 4°$ when electrons energy was 500 MeV. It was placed at the distance of 364 cm from the crystal. The photon beam collimation angle was $\vartheta_c^{PXR} = 1.9$ mrad. The spectrometer efficiency was close to unity in the photon spectral range 50–300 keV. For the 59.4 keV Am^{241} line the detector resolution was $\sigma = 4.8 \pm 0.1$ keV.

Fig. 2(b) shows a typical smoothed instrumental spectrum in the region of maximum radiation yield for $\Theta_B = \Theta_D/2 = 34$ mrad (curve 1) and the background spectrum (curve 2) measured for the (0 0 2) plane of graphite crystal rotated through the angle $\Theta_B \sim= -34$ mrad opposite to the direction of electron beam propagation. The angle Θ_B is counted from the "physical zero" coinciding with the radiation intensity maximum for (0 0 2) planar channeling radiation. The method for the crystal alignment was the same as in [4].

As in [3], well-defined PXR peaks to the third and even fourth reflection orders can be seen for both the pyrolytic graphite crystal. For $\Theta_D = 90°$, no contribution of the (0 0 2) reflection with energy 2.6 keV can be seen. This is caused by the strong photon absorption in the crystal itself and in air on

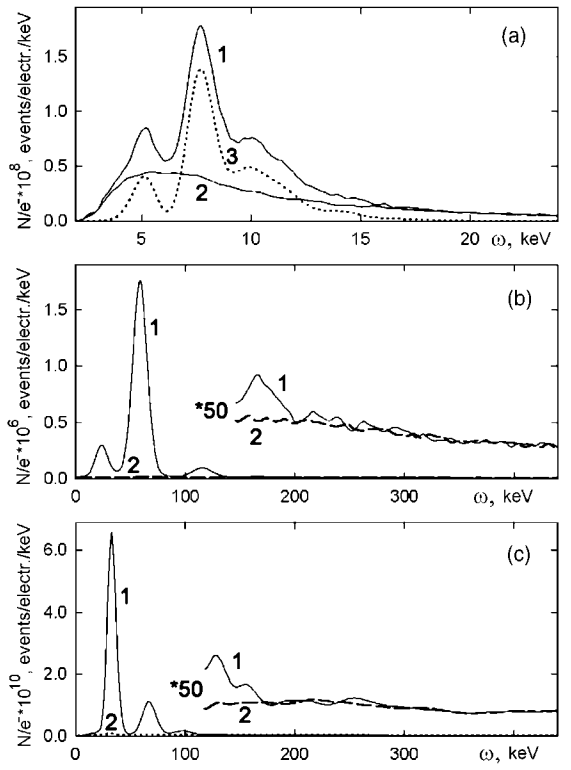

Fig. 2. Experimental radiation spectra. (a) PXR at $\theta_D = 90°$; $E_0 = 900$ MeV. Curves: 1 – experimental spectrum, 2 – background spectrum; 3 – peaks fitted after subtraction of background. (b) PXR at $\theta_D = 4°$; $E_0 = 500$ MeV. Curves: 1 – experimental spectrum, 2 – background spectrum; (c) diffracted photons spectrum from the silicon target. Curves: 1 – for $\Theta_B = 3.59°$ and $\omega_1 = 30$ keV; 2 – $\Theta_B = -4°$ (the background component).

the photon way from the exit window of the synchrotron to the counter. The sharp decrease in the counter efficiency for the photon energy $\omega \geqslant 15$ keV and insufficient energy resolution do not allow one to divide surely close peaks of older PXR orders for this crystal orientation. Nevertheless, a difference between radiation spectra from the crystal and the amorphous targets for photon energies up to $\omega \sim 15$–18 keV indicates that there is a contribution of these reflection orders to the spectrum measured.

For the detector placed at the angle $\Theta_D = 4°$ the peak for the photon energy $\omega \sim 20$ keV is caused by the emission of the fluorescence radiation quanta of iodine when the photons from the (0 0 2) reflection hit the detector. The linear intensity scale used in this figure and relatively large contribution of the continuous background put the contribution of older orders on a mask. However, using of the logarithmic scale as in [4] and fitting of the spectrum measured by the sum of Gaussian curves (see below) show the presence of older reflection orders in the spectrum.

To reduce the statistical errors of the high orders intensity and to correct the drift of the spectrometric instruments gain coefficient, several measurements were performed for each crystal orientation. To find the radiation yield for each reflection order the PXR and the diffracted radiation (see below) experimental spectra were fitted by the sum of Gaussian curves (one curve for each peak) and the background spectrum. Curve 3 in Fig. 2(a) shows the fitting results. To estimate the instrumental error of the results obtained we used the r.m.s. deviation of each reflection order fitted area of individual measurements from its mean values. The method used for spectra measurements and their processing allowed us to define intensity of older reflection orders up to 5–6 with sufficient accuracy.

Fig. 1(b) shows the experiment chart for investigating the soft component of radiation. The electrons accelerated to $E_0 = 500$ MeV intersect $0.52 \times 15 \times 15$ mm^3 a silicon crystal placed in the goniometer. The γ-beam under study passed through the collimator C_1 and two crystal-diffraction spectrometers and was absorbed by Gauss quantometer. The crystal was oriented relative to the electron beam direction using the NaI(Tl) detector which detected photons emitted due to channeling radiation and bremsstrahlung mechanisms with the energies $\omega > 0.5$ MeV, scattered in the convertor Sc. The electron beam parameters, the experimental apparatus and the method of crystal alignment have been described earlier [4,17,18].

To measure the photon yield in a narrow spectral range, two crystal-diffraction spectrometers comprising PG crystals and NaI(Tl) detectors were used. Fig. 1(c) shows the block diagram of the diffractometer.

In these measurements we used two PG crystals. One was the same having been used for the PXR

measurement at $\Theta_D = 4°$. Other crystal with dimensions $3.5 \times 5.5 \times 20$ mm^3 had a greater mosaicity. The mosaic structure distribution in this crystal can also be represented as the sum of two Gaussian distributions with parameters $\sigma_m = 6.2 \pm 0.4$ mrad, $S_1 \sim 0.64 \pm 0.05$ and $\sigma_m = 15.0 \pm 0.1$ mrad, $S_2 \sim 0.36 \pm 0.05$. The distribution centers were shifted by 10 ± 0.3 mrad.

The photon beam passed through the PG crystals placed in the goniometers at the distance ~15.5 m from the target where the radiation under study was generated. The diffracted X-rays (DXR) were detected by the NaI(Tl) spectrometers placed at the distance ~3.5 m from the goniometers where the PG crystals were placed.

The goniometers may be displaced in the horizontal plane to change the observation angle θ_o relative to the electron beam direction within the interval 0–0.1°. In Fig. 1(c) "Beam line" is the initial electron beam direction. For such configuration the crystals $2.5 \times 6.5 \times 22.5$ mm^3 and $3.5 \times 5.5 \times 20$ mm^3 ensured the diffractometers angular capture in the horizontal plane $\Delta\theta_x \sim \pm 0.08$ and $\Delta\theta_x \sim \pm 0.12$ mrad, respectively. For a small angular capture the spectrometer energy resolution is virtually independent on the crystal mosaicity and determined only by the crystal width (2.4 and 3.5 mm, respectively) and the collimation angle of the diffracted beam depending on the collimator C_2. The photon beam collimation angle in the diffraction plane $\Delta\Theta_x = 0.7 \pm 0.05$ mrad ensured the spectrometer resolution $\Delta\omega/\omega = 0.9$–$1.2\%$ as a function of the detector position angle Θ_D. The initial γ-rays collimation angle in the vertical direction was $\theta_y = \pm 0.6$ mrad.

We measured the dependencies of the photon yield with fixed energy on the orientation angle of the silicon crystal axis relative to the electron beam propagation direction and the diffracted photons yield for the selected crystal orientations. To measure the orientation dependencies (OD), we used the detectors of thickness 1 mm, and to measure the yield, we used the NaI(Tl) spectrometer with dimensions $\varnothing\ 63 \times 63$ mm^3. The use of thin NaI(Tl) crystals as detectors and differential discriminators allowed us to register the first diffraction order only. It reduced the background level and allowed obtaining the contribution of background photons with energies differing from the selected one by no more than 1–2%.

By way of example, Fig. 2(c) shows typical smoothed spectra measured with the NaI(Tl) detector of great thickness for two orientations of the pyrolytic graphite crystal. Spectrum 1 was measured in the diffraction curve maximum. The angle between the photon beam incident on the PG crystal and the reflection plane was $\Theta_B = 3.59°$. To correct for the contribution of the background from compton scattered photons in the graphite target itself and scattered radiation background, the crystal was disoriented at the same angle in the opposite direction relative to the photon beam propagation direction (curve 2).

As can be seen from Fig. 2(c), the intensity of the diffracted radiation for the first reflection orders is much greater than that of the background. The diffracted beam intensity becomes less than the background one for the fifth reflection order only. The spectrum and intensity of the diffracted photon beam is completely determined by the incident radiation one, the parameters of the PG crystal used and an experimental setup. Hence, if we measure the diffracted photons spectra for different detector position angles we may obtain information about spectrum of the incident photon beam. In contrast to conventional methods of γ-radiation spectra measurement this method allows investigating the photon spectrum in a very narrow angular cone (far less than γ^{-1}) and gives high energy resolution $\Delta\omega/\omega \sim 1\%$. Contribution of the background from high energy photons emitted into the same angular cone in the spectrum measured is negligible.

The efficiency of the crystal-diffraction spectrometers for different detector position angles Θ_D was calculated in accordance with Eqs. (3)–(10) taking into account the PG crystals dimensions and mosaicity, the spectrometer angular acceptance and the collimation angle of the diffracted photon beam. For the first reflection order the efficiency varied from 3% up to 10%. For the conditions of our experiment, the range of measurable photon energies was $19 \leqslant \omega \leqslant 400$ keV. It was bounded from below by the absorption of photons in air in the path from the accelerator

output window to the NaI(Tl) detectors (~11 m) and from above by the reflectivity of pyrolytic graphite crystals and the minimum detector position angle (~3°).

3.2. Results of the PXR measurements

For calculations we have taken into account the electron beam divergence in the crystals, the real crystals mosaicity, the contribution from the diffraction of the transition radiation and bremsstrahlung, the suppression of bremsstrahlung photon emission due to the medium polarization, the photon absorbtion inside the crystal and the radiation collimation. Secondary reflection of the diffracted radiation (including a diffraction of PXR photons) have been taken into account too.

The obtained experimental data with allowance for the photon absorption in air and in the input window of the NaI(Tl) spectrometer, the efficiency of the detectors and the iodine escape peak for the (0 0 2) reflection order at $\Theta_D = 4°$ coupled with the calculated yield of PXR, the diffracted transition radiation (DTR), and the diffracted bremsstrahlung (DB) for the radiation emission angles $\Theta_D = 90°$ and $\Theta_D = 4°$ are shown in Fig. 3. The ratio of the experimental and calculated total radiation yields $Y_{exp}/Y^{\Sigma}_{calc}$ is shown in Fig. 3(c). The errors are statistical.

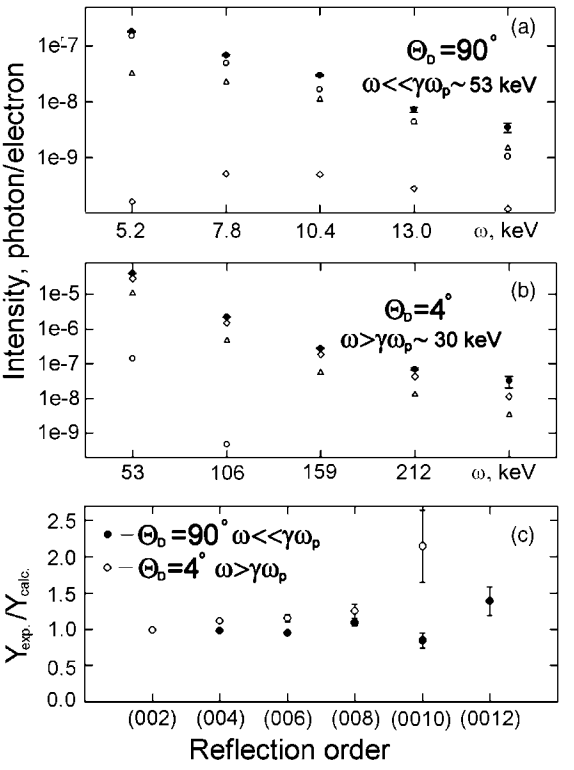

Fig. 3. Dependence of the radiation intensity on the photon energy: experimental spectrum (●) and calculation results of PXR (△), DB (◇) and DTR (○). (a) $\Theta_D = 90°$; (b) $\Theta_D = 4°$; (c) the ratio of the experimental and total (PXR + DB + DTR) calculated radiation yields.

As can be seen from Fig. 3(a), for photons with energy $\omega \ll \gamma\omega_p$ the diffraction of transition radiation photons is the main contribution to the observed spectrum. The bremsstrahlung in this range is virtually completely suppressed by the medium polarization. For the spectral range $\omega > \gamma\omega_p$ the contribution of the diffraction of the real photons is also greater than that of PXR itself by several times (see Fig. 3(b)). Here, DB dominates while DTR contribution is very small, that is caused by the following reasons. Firstly, within this energy range the transition radiation intensity begins to fall as photon energy rises, but since influence of medium polarization effect on BS intensity decreases (see e.g. [7]). Secondly, the TR is generated in front surface of the target only, but the BS is generated throughout thickness of the crystal. The electron multiple scattering angle in the crystal $\sigma_{ms} \sim 5$ mrad is about the crystal mosaicity. Thus the whole BS intensity that can be diffracted in the graphite crystal is much more than TR intensity. This fact results in the big difference between diffracted photons yields from these radiation mechanism. Thirdly, so long as BS is generated along the whole thickness of the crystal the weakening of initial photon beam because of Bragg re-reflection (the secondary extinction effect) has less effect on DB intensity than on DTR one.

As follows from the Fig. 3(c), the experimental data agree with the calculated results for both spectral ranges and all reflection orders observed. For the first reflection orders the discrepancy between experimental yields and the calculated ones are within the statistical errors. For the fifth

reflection order and $\Theta_D = 4°$ the statistical error is very big. Moreover, there are different values of mean-square amplitude of the carbon atoms vibration in PG crystals in the literature. This parameter is very important for the intensity of high order reflection (see Eqs. (2) and (4) in Section 2). As mentioned above, in our calculation we used the PG crystal parameters taken from [2]. If instead of $\langle u_\perp^2 \rangle = 0.014$ Å^2 [2] we take the value of this parameter $\langle u_\perp^2 \rangle = 0.009$ Å^2 from [19], the difference between the experimental and calculated results for the fifth reflection order will reduce. This assumption validity is confirmed by the results of the diffraction measurements. For this diffraction order and all the diffracted spectra measured the obtained initial photon beam intensity is slightly higher than for other ones (see Section 3.3, Fig. 5(a)). The anomalous high intensity of higher reflection orders obtained in experiment [3] is not confirmed by our measurements.

The normalization error of the experimental data presented here does not exceed 10–15%. The calculation error is determined by the error in reproducing the geometry of the measurements, the error in measuring the mosaic crystal structure and approximations used in the calculations. We believe that for the observation angle $\Theta_D = 90°$ the calculation error does not exceed 10%, it increases up to 20% for $\Theta_D = 4°$. This is caused by the specific features of electron hitting at the internal target of the synchrotron. For this observation angle the large crystal face (6.5×22 mm^2) was tilted at a small angle relative to the direction of beam propagation; therefore, the distance along which the electron generates the bremsstrahlung and PXR varies from 6.5 mm to several fractions of a millimeter as a function of the horizontal coordinate of the point at which it strikes the crystal. This increases surely the yield uncertainty of diffracted radiation and PXR.

To check our approach we have calculated photon yield for the experimental conditions of [20]. In the experiment cited for electrons with the energy 900 MeV and the observation angle $\Theta_D = 29.6°$ the emission spectra from a pyrolytic graphite crystal were presented without comparison with calculations, and for the second reflection order the photon yield $Y_2^{exp} = 4.5 \times 10^{-5}$ photon/electron was obtained. Taking into account the bremsstrahlung generation in the air between the synchrotron output window and the target and its diffraction in the PG target the calculated total (PXR + DTR + DB) yield $Y_2^{calc} = 5.1 \times 10^{-5}$ photon/electron was obtained. Taking into account the error of determining the mosaic crystal structure (~10%) and the detection efficiency (~6%), the calculated results well agree with the experimental ones. The ratios of the intensities of the first diffraction orders obtained by fitting of the spectra presented in [20] with allowance for the photon absorption in air and the detector efficiency, $Y_1^{exp}/Y_2^{exp} \sim 1.8$ and $Y_2^{exp}/Y_3^{exp} \sim 4.0$ are very close to the calculated values $Y_1^{calc}/Y_2^{calc} = 1.84$ and $Y_2^{calc}/Y_3^{calc} = 3.79$.

For electrons with energy $E_0 \sim 90$ MeV and a radiation emission angle $\Theta_D = 45°$ a series of the PXR investigations in mosaic PG crystals was carried out in [3,21]. The authors of these works indicated impossibility of description of the obtained experimental results in the frame of kinematic PXR theory. For experimental conditions [3] (the electron energy $E_0 = 90$ MeV and the crystal mosaicity $\sigma_m \approx 3$ mrad) the results of our calculation do not agree with the experimental ones. For the first two reflection orders the measured intensities are much less than the calculated ones, whereas for higher reflection orders the tendency is reversed. The experimental values exceed almost by an order of magnitude the results of our calculations and the PXR calculations carried out in [3] without considering the contribution of the real photons diffraction.

Unlike the experiment [20] and our measurements which were carried out at synchrotrons, the experiment [3] was carried out at the linear accelerator possessing short spill time. Therefore, it is possible that several photons from different electrons were registered as one photon with greater energy. Then a less number of pulses with amplitudes corresponding to the energy of photons of lower orders and a greater number of pulses corresponding to photons of higher reflection orders should be registered in the experiment in comparison with the calculated results, as was reported in [3]. In this case the experimental and calculated

absolute value of the total energy of monochromatic coherent radiation (PXR + DB + DTR) per electron $I = \sum_{i=1}^{n} Y(\omega_i)\omega_i$ should coincide. Here $Y(\omega_i)$ is the number of pulses (photons) per a single electron with amplitude (energy) corresponding to the ith reflection order. The estimation of this quantity based on [3] result led to the value $I_{exp} = 5.87 \times 10^{-5}$ keV/electron, which agreed with the calculated value $I_{calc} = 8.0 \times 10^{-5}$ keV/electron within the normalization error of the cited work results (±40%).

This assumption validity is confirmed by the results of studying the dependence of the PXR intensity for the first reflection order on the mosaic graphite crystal structure performed more recently at the same facility [21]. Under similar experimental conditions ($E_0 = 99$ MeV, $\sigma_m = 3.3$ mrad and the same observation angle), the ratio of the measured and calculated photon yields of the first reflection order ($\omega_1 = 4.88$ keV) increased from ~0.25 [3] up to ~0.5 [21]. For the electron energy $E_0 = 99$ MeV and the crystal mosaicity $\sigma_m = 3.3$ mrad experimental result [21] $Y_{exp} = 7.5 \times 10^{-6}$ photon/electron agrees satisfactorily with our calculated result $Y^{\Sigma}_{calc} = 10.2 \times 10^{-6}$ photon/electron within the normalization error (±40%). Nearly the same overestimation of the calculated results compared to the experimental data (~25–30%) was obtained for other graphite crystals examined in the work cited.

Depending on the experimental conditions the photon diffraction in mosaic crystals may not only increase the total emission yield (PXR + DB + DTR) compared to the PXR intensity without considering the real photons diffraction, as in our measurements, but also decrease it. In the experiments [3,21] the contribution of the bremsstrahlung photons diffraction was very small because of strong absorption of the first reflection order photons. For electrons with energy $E_0 \sim 90$ MeV the transition radiation intensity also decreases sharply in this spectral range. Therefore, for the experiment [21] the measured photon yield $Y_{exp} = 7.5 \times 10^{-6}$ photon/electron and the total calculated intensity of the first reflection order $Y^{\Sigma}_{calc} = 10.2 \times 10^{-6}$ photon/electron were found to be less than the PXR photon yield calculated without considering the PXR photon diffraction $Y^{PXR}_{calc} = 12.1 \times 10^{-6}$ photon/electron, as was noted in the work cited.

3.3. Measurements of bremsstrahlung and channeling radiation spectra

The orientation dependences (OD) measurements of the soft radiation yield in the silicon crystal [22] showed that the radiation contribution of the planar channeling radiation was not more than 25% from the incoherent background (the bremsstrahlung plus transition radiation) in the energy range $\omega \sim 30$–50 keV. With electrons moving at small angles to the crystallographic axis, the radiation yield increases almost by an order of magnitude. At large angles with respect to the axis and outside of the planar channeling mode, the radiation yield in the X-ray energy range was independent on the crystal orientation [14,22].

For the intersection with the ⟨1 1 0⟩ axis the OD measurements carried out for photon energies lying in the range $19 \leqslant \omega \leqslant 72$ keV and observation angles $\theta_o \leqslant \theta_o^{max} = 1.7$ mrad ($\theta_o^{max} > \gamma^{-1} > \psi_c$, where $\psi_c = 0.66$ mrad is the critical angle of the ⟨1 1 0⟩ axial channeling of 500 MeV electrons in the silicon crystal) have shown that the maximum in the ODs is observed exactly when the crystallographic axis coincides with the direction toward the crystal analyzer of the difractometer.

By way of example, Fig. 4 illustrates the OD of radiation under the following conditions: $\theta_o = 0 \pm 0.1$ mrad, $\theta_y = 0.6$ mrad, and $\theta_x = \pm 0.6$ mrad (Fig. 4(a)) and $\theta_o = 1.2 \pm 0.1$ mrad, $\theta_y = 0.6$ mrad and $\theta_x = \pm 1.5$ mrad (Fig. 4(b)). Here θ_y and θ_x specify the collimator aperture for measuring total radiation energy and compton scattered photon yield for energies $\omega \geqslant 0.5$ MeV (curves 1 and 2, respectively). Curves 3 and 4 show the OD of the yield of photons with energy $\omega = 29$ and 36.5 keV, respectively. It is evident from the figure that a change of the observation angle results in decrease of the examined radiation intensity and the displacement of the OD maximum proportional to the change of the observation angle. The peak/pedestal ratio for both photon energies remains approximately the same.

The width of the peak (FWHM) of X-ray photon yield orientation dependence ($\Delta\Theta \sim 2.5$ mrad)

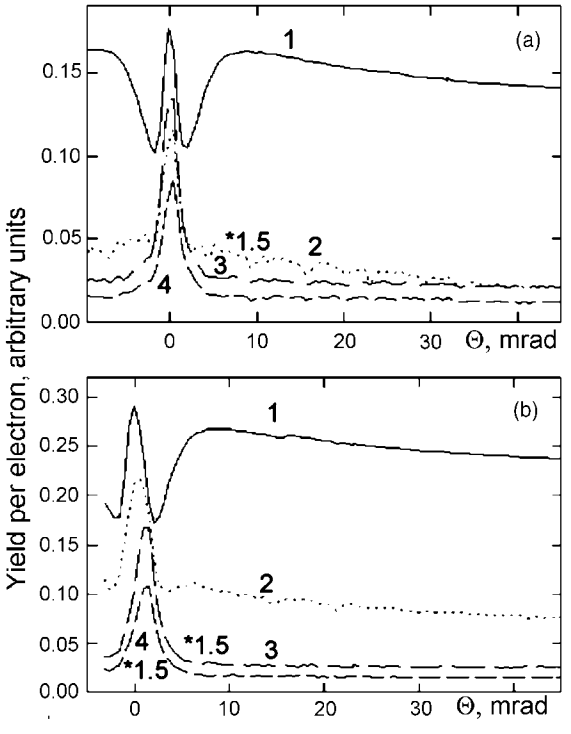

Fig. 4. Orientation dependences of the photon yield: silicon crystal with ⟨1 1 0⟩ orientation; $t = 0.52$ mm; $E_0 = 500$ MeV. 1 – total radiation energy; 2 – $\omega \geqslant 0.5$ MeV; 3 – $\omega = 29$ keV; 4 – $\omega = 36.5$ keV. (a) $\alpha = 0$; $\theta_o \sim 0$ mrad; $\Delta\theta_o = \pm 0.1$ mrad; $\theta_x = \pm 0.6$ mrad; (b) $\alpha = 0$; $\theta_o \sim 1.2$ mrad; $\Delta\theta_o = \pm 0.1$ mrad; $\theta_x = \pm 1.5$ mrad.

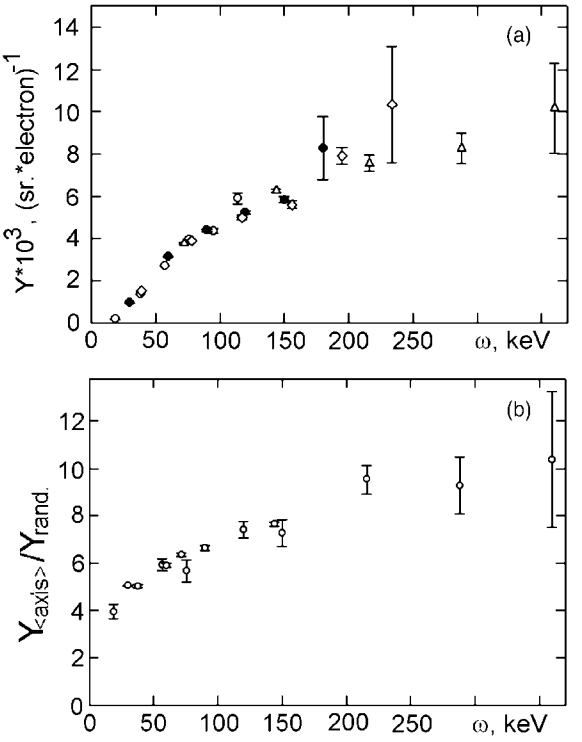

Fig. 5. (a) Spectrum of the angular density of the ⟨1 1 0⟩ channeling radiation intensity for four detection angles: ○ – $\Theta_D = 11.16°$ and $\omega_1 = 19$ keV; ● – $\Theta_D = 7.18°$ and $\omega_1 = 30$ keV; ◇ – $\Theta_D = 5.58°$ and $\omega_1 = 39$ keV; △ – $\Theta_D = 2.94°$ and $\omega_1 = 72$ keV; (b) The ratio of the radiation yields for disoriented and oriented crystals.

is larger than that for the OD peak of total radiation energy ($\Delta\Theta \approx 1.8$–2.0 mrad) and than the doubled value of the critical angle of the ⟨1 1 0⟩ axial channeling ψ_c. It is well known (see, for example [5,6]) that the radiation intensity of particles captured in the axial channeling regime sharply decreases for photons with energy much less than the characteristic one (for our conditions, $\omega_m \sim 5$ MeV). Therefore, it seems likely that the radiation not axially channeled but above barrier electrons was observed in the experiment. According to [5] this radiation intensity in thick crystals is as high as the channeling radiation intensity and the spectrum shape in the soft energy region should be close to that of the bremsstrahlung spectrum.

Fig. 5(a) shows the spectral dependence of the angular density of radiation intensity $Y = \Delta N(\omega)/\Delta\Omega/P(\omega)$ as measured by the crystal-diffraction spectrometer for electrons incident along the ⟨1 1 0⟩ crystallographic axis of the silicon crystal (Fig. 5(a)). Here $\Delta N(\omega)$, $\Delta\Omega$ and $P(\omega)$ are the number of photons in the diffraction spectrum with energy ω, solid angle, and efficiency of the diffractometer, respectively. The ratio of the angular densities of the radiation intensity for the oriented and disoriented crystals is shown in Fig. 5(b). The observation angle is $\theta_o = 0$, that is the graphite crystals are placed along the direction of incident electron beam.

The measurements were carried out for two positions of each diffractometer covering the following energy ranges (ω_1–ω_5): 19–85 keV (○), 30–150 keV (●), 39–195 keV (◇) and 72–360 keV (△). As can be seen from Fig. 5(a), for the similar photon energies, as for example, 72 keV (△),

76 keV (○) and 78 keV (◇), the values of the angular density of radiation intensity measured at different diffraction angles agree within the experimental error. The smooth increase of the angular density of radiation intensity in the spectral range 19–150 keV is well reproduced in all measurements. This confirms the validity of the emission spectrum measurement technique we employed.

From Fig. 5(b) it can be seen that the radiation intensity generated by electrons moving along the ⟨1 1 0⟩ axis is much greater than that generated by electrons over the disoriented crystal over the entire range of examined energies. The emission spectra shapes do not coincide for oriented and disoriented crystals. The ratio of the radiation intensities increases smoothly from ~4 for photons with energy from 19 up to ~10 for $\omega = 360$ keV. We believe that this fact testifies the suppression presence for both incoherent radiation (the Ter-Mikaelian effect) and coherent one.

For the disoriented crystal the intensity spectrum in the first approximation can be considered as the bremsstrahlung spectrum in an amorphous matter. The measured spectrum from the disoriented silicon crystal is shown in Fig. 6. For photon energy $\omega = 30$ keV $\sim \gamma\omega_p$ ($\omega_p \approx 32$ eV) the radiation intensity decreases approximately by a factor four in a comparison with larger photon energies. Presented also here are two calculated curves. In calculation, the change of the angular distribution of electrons passing through the crystal and the photon absorption inside the target were taken into account. The curve 1 was calculated without taking into account the dependence of the bremsstrahlung suppression because of the density effect on photon emission angle. The similar dependence was examined in recent experiments at SLAC at electron energies 8 and 25 GeV [10]. The curve 2 was calculated taking into account the influence of the photon emission angle on the bremsstrahlung suppression, according to [23].

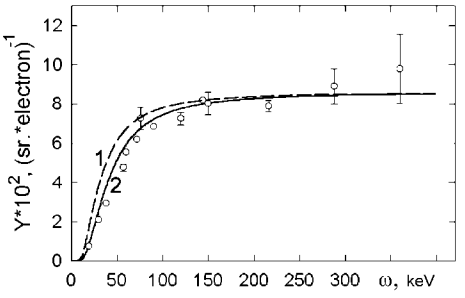

Fig. 6. Spectrum of the angular density of the radiation intensity for the disoriented crystal: ○ – experiment, the curves – calculation: 1 – without angular dependence of the bremsstrahlung suppression, 2 – angular dependence of the bremsstrahlung suppression is taken into account.

Because a scraper [16] was used in the experiment to decrease the multitraversal of electrons through the thin target and the error in measuring the accelerator current was approximately 10–15%, the experimental and calculated spectra were normalized to the ratio between measured and calculated values of the bremsstrahlung total energy in the collimator with aperture $\vartheta_c = 0.6$ mrad ($\Delta E_{rad}^{exp} = 0.156$ MeV/electron and $\Delta E_{rad}^{calc} = 0.217$ MeV/electron). With allowance for this correction, the absolute values of the experimental and calculated intensities for photons with energies $\omega \geqslant 100$ keV agree well.

From the Fig. 6 one can see that here we observe a very clear bremsstrahlung suppression. The curve 2 describes the experimental points better than curve 1. Nevertheless, for the photon energy less than 100 keV the experimental points are placed slightly lower than calculated curve. The most likely reason of the difference between the calculated bremsstrahlung yield and the measured one is an additional contribution of the bremsstrahlung suppression due to the Landau–Pomeranchuk–Migdal effect [8]. However, in contrast to results of SLAC experiments [9,10] for electron energy 500 MeV and a silicon target, the bremsstrahlung suppression due to medium polarization effect is predominant.

4. Search for a more effective source of X-radiation

Search for the monochromatic X-ray radiation source with the photon energy $\omega \approx 33.1$ keV (for medicine purposes such as digital subtractive angiography) is subject of many studies (see, for example [20]). Therefore, it is interesting to compare the PXR intensity at this photon energy for a perfect crystal and a mosaic PG crystal.

For comparing a diamond crystal was taken as the photon absorption dependence on the radiation frequency was identical for both crystals. The electron energy was 150 MeV, because the bremsstrahlung suppression due to medium polarization effect in the examined spectral range is disappeared and the characteristic radiation angle ($\gamma^{-1} \approx 3$ mrad) is close to typical mosaicity value of the PG crystals ($\sigma_m \sim 3$ mrad). For the same reason the X-ray emission collimation angle was equal to 3 mrad. The PXR calculation results for the (1 1 1) reflection in the diamond and at the angle $\Theta_B = 5.22°$ (curve 1) and in the (0 0 2) reflection of the PG crystal and at the angle $\Theta_B = 3.2°$ (curve 2) are given in Fig. 7(a). Curve 3 is the calculated PXR spectrum for the (0 0 2) reflection in the "perfect" PG crystal.

For comparing the (1 1 1) reflection in the diamond was chosen as according to the PXR theory the photon yield for this reflection is the most intensive. For the mosaic PG crystal the PXR diffraction was taken into account. The crystal thickness along the electrons propagation direction ($t = 1$ mm and $t = 0.64$ mm, respectively for the graphite and the diamond) was chosen so that the number of atoms in both targets was identical.

It is evident from the figure, that the PXR spectral density for the diamond is almost twice lower than that for the mosaic PG crystal, which is approximately twice lower, than for the perfect graphite crystal. A small width of the PXR spectral line for the diamond is caused by the large Bragg angle. According to well known dependence $\Delta\omega/\omega \sim \vartheta_c \cdot \cos(\Theta_B)/\sin(\Theta_B)$, for the same collimation angle, the increase of the Bragg's angle results in narrowing the PXR spectral line. In the collimator aperture the radiation yield was approximately 5 and 7 times less for the diamond, than for the mosaic and perfect graphite crystals. It is due to larger interplanar distance in the graphite crystal. According to the PXR theory the radiation intensity is proportional to a square of Fourier-component of the electron density distribution in the crystal atom $f^2(\vec{g}) \sim |g|^{-2}$, where $|g| = 2\pi \cdot \sqrt{I_1^2 + I_2^2 + I_3^2}/A$. The lattice parameters for the diamond and graphite are $A_{di} = 0.356$ nm and $A_{PG} = 0.67$ nm, respectively. Therefore, the

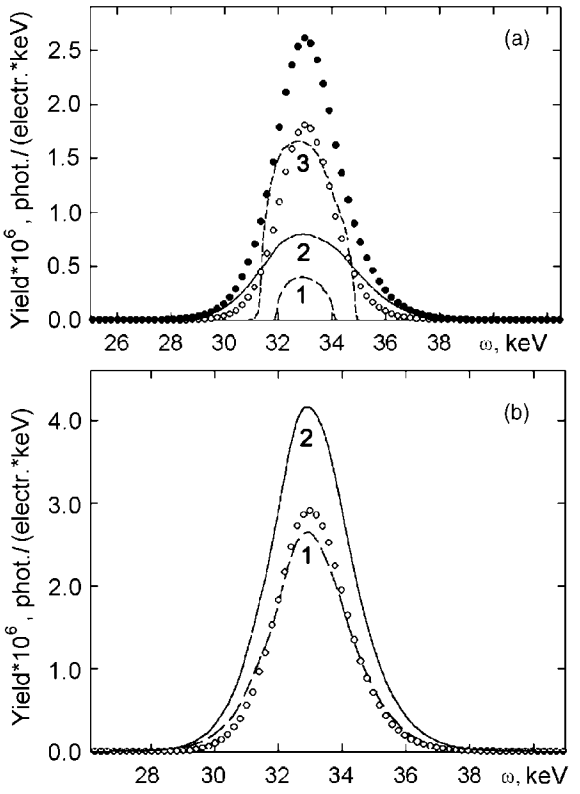

Fig. 7. Calculated radiation spectra for $E_0 = 150$ MeV and $\vartheta_c = 3$ mrad: (a) diamond and pyrolytic graphite crystals: 1 – PXR, diamond, (1 1 1), $t = 0.64$ mm, $\Theta_B = 5.22°$; 2 – PXR, graphite, (0 0 2) $t = 1$ mm, $\sigma_m = 3$ mrad, $\Theta_B = 3.2°$; 3 – PXR, perfect graphite, (0 0 2) $t = 1$ mm, $\Theta_B = 3.2°$; ○ – DB, ● – DB + PXR, graphite, (0 0 2) $t = 1$ mm, $\sigma_m = 3$ mrad, $\Theta_B = 3.2°$. (b) Silicon and pyrolytic graphite crystals: 1 – DB + PXR, graphite, (0 0 2) $t = 1$ mm, $\sigma_m = 3$ mrad, $\Theta_B = 3.2°$; 2 – DB + PXR, compound Si + PG target; ○ – diffracted bremsstrahlung from the silicon target.

PXR intensity from the graphite is much higher than that from the diamond.

Comparing the spectra for the mosaic and perfect graphite crystals one can see that the crystal mosaicity leads to decrease of the radiation intensity, if the radiation collimator is used, and to increase of the spectral line width of the radiation observed. The PXR spectral density is more than twice lower due to the mosaicity presence. The radiation yield decreases from 4.57×10^{-6} photon/electron down to 3.36×10^{-6} photon/electron, that is about 1.5 times.

As was shown in Section 3 (see also [4,13]), the mosaicity causes to an additional contribution of diffraction of the transition radiation and bremsstrahlung real photons. The DB yield (○) for this crystal thickness ($Y^{DB} = 4.69 \times 10^{-6}$ photon/electron) is comparable with the PXR yield from the perfect graphite crystal. Thus the total radiation intensity (PXR + DB) from the mosaic graphite crystal is approximately 1.5 times greater than the radiation intensity from the perfect graphite crystal and 6–7 times higher than the PXR intensity from the diamond. As the crystal thickness increases up to the photon absorption length (if secondary extinction is taken into account, it is about 10–12 mm), the contribution of DB continues to build up. This growth is due to increase of the reflectivity and bremsstrahlung yield with increasing the PG crystal thickness. Therefore the total radiation yield from a thick PG crystal for electron energy 100–150 MeV is about order of magnitude greater than that from a diamond, or another perfect crystal of the same thickness.

In recent years the PXR generation in the so-called X-ray mirror is intensively examined. The X-ray mirror consisted of 300 layer pairs (W/B_4C) was used in the experiment [24]. The electron energy was equal to 500 MeV. With the mirror of total thickness of 0.37 μm, the angular density of the radiation yield about 0.22 photon/electron/sr was obtained at $\omega = 15$ keV and the detector position angle $\Theta_D \approx 4°$. For the 1 mm thick PG crystal, the detector position angle $\Theta_D \approx 18.2°$, and the electron energy $E_0 = 900$ MeV the angular density of the radiation yield $dN/d\Omega^{PG}_{exp} = (0.46 \pm 0.07)$ photon/electron/sr was obtained in experiment [25]. In the experiment cited above the electron beam hits near the edge of the target, hence the "true" electron path in the crystal is unknown. For the whole crystal thickness along the electron beam direction (~0.03 rad. length) our calculation has given the value $dN/d\Omega^{PG}_{calc} = 1.94$ photon/electron/sr, i.e., almost an order of magnitude higher than in the experiment [24].

Our estimations show that for a thin X-ray mirror [24] the angular density of the radiation yield per unit radiation length is almost twice as that for a thick PG crystal [25]. However, the increase of the X-ray mirror thickness is a complicated technological problem. Moreover, the X-ray mirror thickness increase results in broadening the electron beam in the target so the PXR yield increases slower than the X-ray mirror thickness. At last, generation of hard photons $\omega \sim 30$ keV with X-ray mirror requires a very small PXR emission angle ($\Theta_D \sim 2°$). For thick targets and moderate electron energies (~several hundreds MeV) the increase in mirror thickness leads to overlapping of the PXR photon beam and bremsstrahlung one (see e.g. [26]). In other words, for these conditions (an electron and photon energies) a PG crystal is a better emitter of monochromatic X-ray than a thick X-mirror.

Another way to increase a total yield of monochromatic X-rays is to use a compound target. It means that the target consists of layers of different materials. One layer is for the photon beam generation and the second layer is for the photon diffraction. A similar method was used for X-ray generation in the experiment [20]. The authors of that paper used a stack of silicon plates for generation of transition radiation and pyrolytic graphite for diffraction of the resulting radiation. The transition radiation intensity is known to fall down sharply when the photon energy ω becomes greater than $\omega = \gamma\omega_p$. Therefore for the electron energy less than 1 GeV and photon energy about 30 keV the efficiency of this X-ray generation mechanism decreases drastically [27].

The bremsstrahlung and channeling radiation (see Section 3.3) are more intensive in the above mentioned experimental conditions. In our calculation the compound target consists of two layers: the 0.5 mm thick silicon target (as in our experiment) and, as in previous calculations, the PG crystal with mosaicity $\sigma_m = 3$ mrad. The other conditions are the same as in previous calculations.

The results of calculations of the X-ray spectra for such a compound target are given in Fig. 7(b). One can see that the radiation yield from the compound target Si + PG (curve 2) is more than 1.5 times greater, than from single PG crystal (curve 1): 13.4×10^{-6} photon/electron and 8.36×10^{-6} photon/electron, respectively. The bremsstrahlung radiation yield generated by relativistic electron beam in the silicon target and diffracted in the PG crystal (○) is comparable with the total

(PXR + DB) yield from the single graphite crystal. In calculating the PXR and DB yield in the compound target (curve 2) we have taken into account the divergence increase of the electron beam hitting the graphite.

If the first layer is an axially aligned crystal, the photon beam is generated by bremsstrahlung and axial channeling radiation mechanisms. The channeling radiation is far more intensive in this spectral range and has more narrow angular distribution than the bremsstrahlung, therefore, the total yield of the diffracted radiation from such a compound target will be considerably greater. In the experiment [28] for the electron energy 300 MeV and the 0.5 mm thick diamond crystal, an intensity of the $\langle 100 \rangle$ channeling radiation was about 25 times higher than bremsstrahlung one. Therefore for this electron energy, the X-ray enhancement is supposed to be about fivefold in comparison with using an amorphous target as the radiation emitter. In any case for the electron energy about several hundreds MeV the diffracted photons yield for this compound target will be much higher than the PXR yield for any crystal of similar thickness.

5. Conclusion

1. The contribution of real photon diffraction being taken into account, the PXR theory in kinematic approximation describes well the experimental results with mosaic pyrolytic crystals.
2. For the spectral region $\omega \geqslant \gamma\omega_p$, the emission from the axial channeled electrons is far more intensive than the bremsstrahlung and transition radiation.
3. Comparison between the calculated photon yield in the mosaic PG crystal and in the perfect diamond crystal has shown that the mosaic PG crystal provides far more intensive quasimonochromatic photon beam.
4. More intensive X-radiation yield may be obtained using compound target; the first target is for the photon generation, the second one (PG crystal) is for the photon diffraction. Using an axially aligned crystal as the first target may provide more intensive and monochromatic hard X-ray beam than ordinary amorphous target.

Acknowledgement

The work has been partially supported by Russian Fund for Basic Research under the contract N 01-02-17471.

References

[1] V. Arkadiev, H. Brauninger, W. Burkert, A. Bzhaumikhov, H.-E. Gorny, N. Langhoft, A. Oppitz, J. Rabe, Nucl. Instr. and Meth. A 455 (2000) 589.

[2] M. Chabot, P. Nicolai, K. Wohrer, J.P. Rozet, A. Touati, A. Chetioui, D. Vernhet, Nucl. Instr. and Meth. B 61 (1991) 377.

[3] R. Fiorito, D.W. Rule, K.L. DiNova, X.K. Maruyama, S.J. Evertson, M.J. Osborne, D. Snyder, H. Rietdyk, M.A. Piestrup, A.H. Ho, Phys. Rev. Lett. 71 (1993) 704.

[4] O.V. Chefonov, B.N. Kalinin, G.A. Naumenko, D.V. Padalko, A.P. Potylitsyn, I.E. Vnukov, I. Endo, M. Inoue, Nucl. Instr. and Meth. B 173 (2001) 18.

[5] V.A. Bazylev, N.K. Zhevago, Radiation of Relativistic Particles in External Fields and in Matter, Nauka, Moscow, 1987 (in Russian).

[6] M.A. Kumakhov, R. Wedell, Radiation of relativistic light particles during interaction with single crystals, Spectrum Physics, Heidelberg, 1991.

[7] M.L. Ter-Mikaelian, High-Energy Electromagnetic Processes in Condensed Media, Wiley-Interscience, New York, 1972.

[8] L.D. Landau, I.Ya. Pomeranchuk, Dokl. Akad. Nauk SSSR 92 (1953) 735.

[9] P.L. Anthony, R. Becker-Szendy, P.E. Bosted, M. Cavalli-Sforza, L.P. Keller, L.A. Kelley, S.R. Klein, G. Niemi, M.L. Perl, L.S. Rochester, J.L. White, Phys. Rev. Lett. 75 (1995) 1949.

[10] P.L. Anthony, R. Becker-Srendy, P.E. Bosted, M. Cavalli-Sforza, L.P. Keller, L.A. Kelley, S.R. Klein, G. Niemi, M.L. Perl, L.S. Rochester, J.L. White, Phys. Rev. Lett. 76 (1995) 3350.

[11] H. Nitta, Phys. Lett. A 158 (1991) 270.

[12] R. James, The optical principles of the diffraction of X-rays, G. Bell and Sons, London, 1958.

[13] I.E. Vnukov, B.N. Kalinin, G.A. Naumenko, D.V. Padalko, A.P. Potylitsyn, Russ. Phys. J. 44 (2001) 263.

[14] I.E. Vnukov, B.N. Kalinin, A.A. Kiryakov, G.A. Naumenko, D.V. Padalko, A.P. Potylitsyn, Russ. Phys. J. 44 (2001) 281.

[15] S. Suzuki, T. Tsuru, T. Katayama, M. Kobayashi, S. Iwata, Nucl. Instr. and Meth. 111 (1973) 39.
[16] B.N. Kalinin, A.A. Kurkov, A.P. Potylitsyn, Russ. Phys. J. 44 (1991) 535.
[17] Yu.N. Adishchev, S.A. Vorob'ev, V.N. Zabaev, B.N. Kalinin, A.A. Kurkov, A.P. Potylitsyn, Sov. J. Nucl. Phys. 35 (1982) 63.
[18] B.N. Kalinin, E.I. Konovalova, G.A. Pleshkov, A.P. Potylitsyn, V.M. Tarasov, V.K. Tomchakov, I. Khakberdiev, Instrum. Exp. Tech. 28 (1985) 533.
[19] R. Chen, P. Trucano, Acta Cryst. A 44 (1978) 396.
[20] Y. Takashima et al., Nucl. Instr. and Meth. B 145 (1998) 25.
[21] R.B. Fiorito, D.W. Rule, C.A. Martin, W.M. Buckingham, L.R. Ivey, K.L. DiNova, X.K. Maruyama, M.A. Piestrup, in: Proc. Second Int. Symposium on Radiation of Relativistic Electrons in Periodical Structures, Tomsk 1995, Eds. Yu.L. Pivovarov and A.P. Potylitsyn, Cambridge Interscience Publishing, 1996.
[22] B.N. Kalinin, G.A. Naumenko, D.V. Padalko, A.P. Potylitsyn, I.E. Vnukov, Nucl. Instr. and Meth. B 173 (2001) 253.
[23] V.P. Kleiner, N.N. Nasonov, N.A. Shlyahov, Ukr. Phys. J. 37 (1992) 48 (in Russian).
[24] V.V. Kaplin, S.R. Uglov, V.N. Zabaev, M.A. Piestrup, C.K. Gary, Appl. Phys. Lett. 76 (2000) 3647.
[25] K.Yu. Amosov et al., JETP Lett. 60 (1994) 518.
[26] T. Akimoto, M. Tamura, J. Ikeda, et al., Nucl. Instr. and Meth. A 459 (2001) 78.
[27] K. Chouffani, M.Yu. Andreyashkin, I. Endo, J. Masuda, T. Takahashi, Y. Takashima, Nucl. Instr. and Meth. B 173 (2001) 241.
[28] A.S. Balayan, B.N. Kalinin, G.A. Naumenko, A.P. Potylitsyn, V.P. Sarychev, I.E. Vnukov, Phys. Lett. A 159 (1991) 433.